Journal of Enzyme Inhibition and Medicinal Chemistry

ISSN: 1475-6366 (Print) 1475-6374 (Online) Journal homepage: informahealthcare.com/journals/ienz20

Novel furfurylidene *N*-acylhydrazones derived from natural safrole: discovery of LASSBio-1215, a new potent antiplatelet prototype

Ana Paula C. Rodrigues, Luciana M.M. Costa, Bruna L.R. Santos, Rodolfo C. Maia, Ana L.P. Miranda, Eliezer J. Barreiro & Carlos A.M. Fraga

To cite this article: Ana Paula C. Rodrigues, Luciana M.M. Costa, Bruna L.R. Santos, Rodolfo C. Maia, Ana L.P. Miranda, Eliezer J. Barreiro & Carlos A.M. Fraga (2012) Novel furfurylidene *N*-acylhydrazones derived from natural safrole: discovery of LASSBio-1215, a new potent antiplatelet prototype, Journal of Enzyme Inhibition and Medicinal Chemistry, 27:1, 101-109, DOI: 10.3109/14756366.2011.578575

To link to this article: https://doi.org/10.3109/14756366.2011.578575

Journal of Enzyme Inhibition and Medicinal Chemistry, 2012; 27(1): 101–109

ISSN 1475-6366 print/ISSN 1475-6374 online
DOI: 10.3109/14756366.2011.578575

informa
healthcare

RESEARCH ARTICLE

Novel furfurylidene *N*-acylhydrazones derived from natural safrole: discovery of LASSBio-1215, a new potent antiplatelet prototype

Ana Paula C. Rodrigues[1,2], Luciana M.M. Costa[1,3], Bruna L.R. Santos[1,4], Rodolfo C. Maia[1,2], Ana L.P. Miranda[1,3,4], Eliezer J. Barreiro[1,2,4], and Carlos A.M. Fraga[1,2,4]

[1]Laboratório de Avaliação e Síntese de Substâncias Bioativas (LASSBio), Faculdade de Farmácia, Universidade Federal do Rio de Janeiro, Rio de Janeiro, RJ, Brazil, [2]Programa de Pós-Graduação em Química, Instituto de Química, Universidade Federal do Rio de Janeiro, Rio de Janeiro, RJ, Brazil, [3]Programa de Pós-Graduação em Ciências Farmacêuticas, Faculdade de Farmácia, Universidade Federal do Rio de Janeiro, Rio de Janeiro, RJ, Brazil, and [4]Programa de Pós-Graduação em Farmacologia e Química Medicinal, Instituto de Ciências Biomédicas, Universidade Federal do Rio de Janeiro, Rio de Janeiro, RJ, Brazil

Abstract

We describe herein the discovery of (*E*)-*N*-methyl-*N*'-((5-nitrofuran-2-yl)methylene)benzo[*d*][1,3]dioxole-5-carbohydrazide (**9e**), named LASSBio-1215, as a novel antiplatelet agent belonging to the *N*-methyl-*N*-acylhydrazone class, which exert their antiaggregating actions on human and rabbit platelets induced by different agonists, through cyclooxygenase-1 (COX-1) or thromboxane synthase inhibition. This compound was elected after screening of a series of functionalized furyl *N*-acylhydrazone derivatives, synthesized from natural safrole **10**. I*n vitro* assays showed that compound **9e** presents platelet-aggregating activity in rabbit platelet-rich plasma (PRP) induced by arachidonic acid (IC_{50} = 0.7 μM) and collagen (IC_{50} = 4.5 μM). Moreover, LASSBio-1215 also inhibited almost completely the second wave of adenosine diphosphate-induced platelet aggregation in human PRP, and this effect was correlated with their ability to block the production of pro-aggregating autacoid thromboxane A_2.

Keywords: *N*-acylhydrazone, 1;3-benzodioxole, *N*-methyl-*N*-acylhydrazone, antiplatelet drugs, COX inhibitors

Introduction

Platelet activation and aggregation are crucial events to the pathophysiology of several acute and chronic arterial vascular diseases that are responsible for important impact on morbidity, mortality, and health care costs worldwide[1,2]. Despite the worrying status of these pathological states associated with thrombus formation, the currently available therapies are limited to few antiplatelet drugs[3] belonging to one of these four main classes: (i) cyclooxygenase-1 (COX-1) inhibitors, for example, aspirin **1**; (ii) adenosine diphosphate (ADP) receptor antagonists, represented by thienopyridine derivatives as clopidogrel **2**; (iii) glycoprotein IIB/IIIA receptor antagonists, for example, tirofiban **3**; (iv) selective phosphodiesterase 3 inhibitors, for example cilostazol **4** (Figure 1). All of them presented therapeutic limitations, for example reduced oral effectiveness[4], characteristic side effects such as bleeding or are able to induce resistance after long-term treatment[5].

In this context, we have described previously the platelet antiaggregating profile of a series of 2-pyridynylhydrazones **5**[6] and *N*-acylhydrazone (NAH) derivatives from phenothiazine **6**[7] and 1,3-benzodioxolyl series, for example LASSBio-294 **7** and LASSBio-785 **8**[8], which

Address for Correspondence: Prof. Carlos Alberto Manssour Fraga, Laboratório de Avaliação e Síntese de Substâncias Bioativas (LASSBio), Faculdade de Farmácia, Universidade Federal do Rio de Janeiro, P.O. Box 68.023, 21941-902, Rio de Janeiro, RJ, Brazil. Tel: +55-21-25626503. Fax: +55-21-2562–6503. E-mail: cmfraga@ccsdecania.ufrj.br

(Received 29 October 2010; revised 28 March 2011; accepted 04 April 2011)

have also potent inotropic[9] and vasodilator properties[10,11] (Figure 2).

The NAH subunit has been described as the pharmacophoric framework of several bioactive substances from different therapeutic classes[12,13], indicating the privileged status of this moiety, as has been recently reviewed[14].

So, in the scope of a research program aiming to design, synthesize, and perform the pharmacological evaluation of new platelet antiaggregating lead-compound candidates, we developed new functionalized furyl 1,3-benzodioxolyl-*N*-acylhydrazone derivatives **9** (Figure 2), designed as isosteres of the antiplatelet thienyl-NAH derivatives **7** and **8**.

These target compounds **9a–j** were planned by insertion of the furane ring present in antiplatelet derivatives **5** and **6** at the imine subunit of 1,3-benzodioxolyl-NAH derived from Brazilian natural product safrole **10**[15]. In

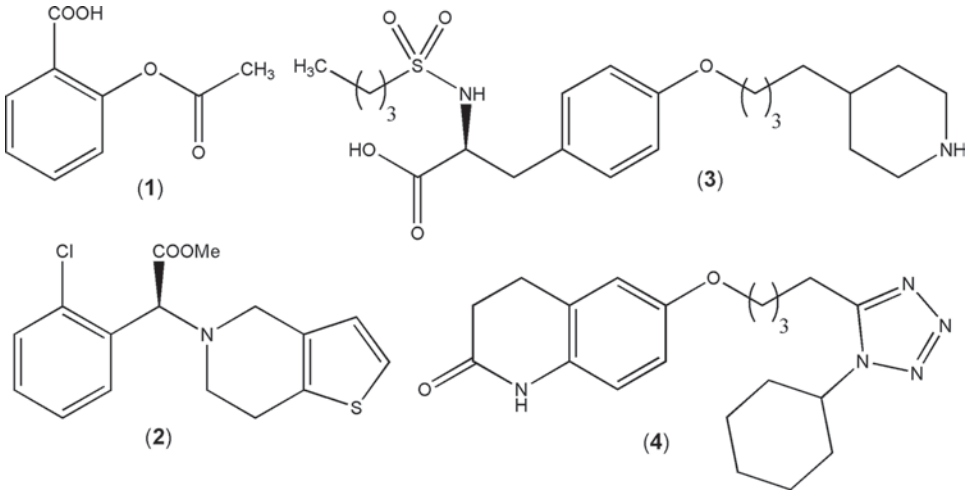

Figure 1. Currently available platelet antiaggregating drugs.

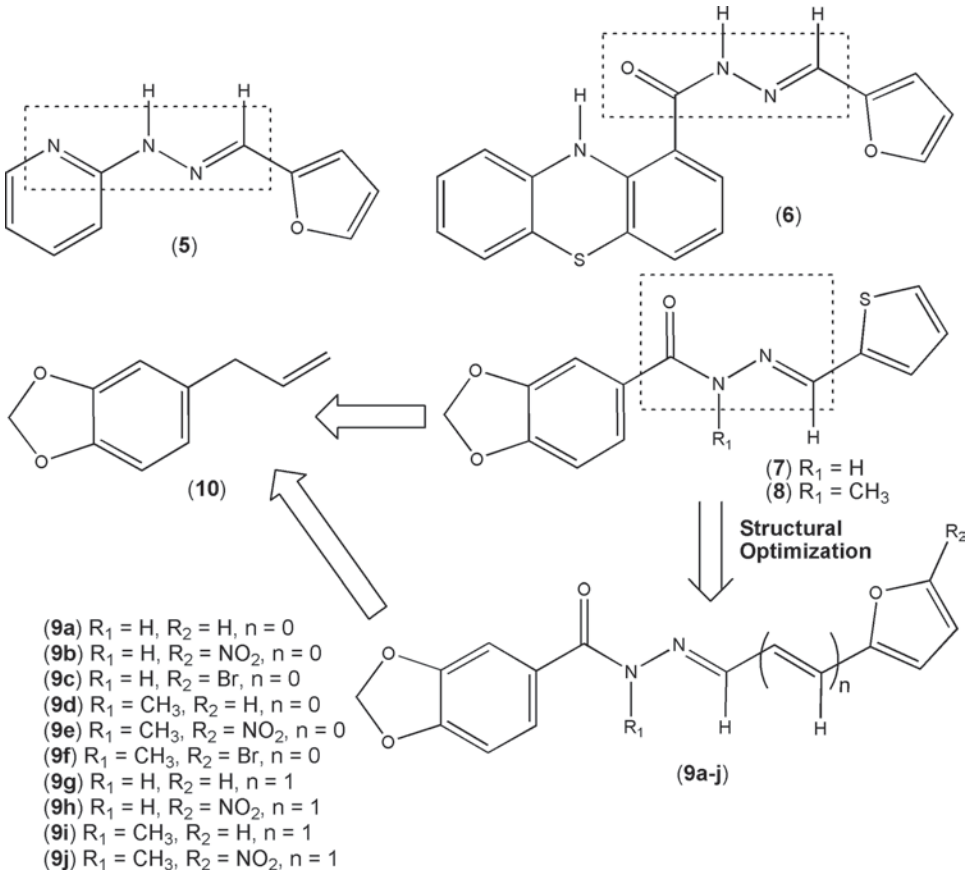

Figure 2. Design concept of new functionalized furylydene 1,3-benzodioxolyl-*N*-acylhydrazine derivatives **9a–f** and the vinylogous analogues **9g–j**.

order to define the structure–activity relationships based on steric, electronic, and lipophilic effects of substituents at *C5*-position of the furane subunit, we proposed the substitution of the hydrogen by bromine and nitro groups (Figure 2). In addition, considering the well-known conformational effects promoted by methylation of the amide group at NAH moiety[11], we decided to prepare the corresponding *N*-methyl-NAH derivatives **9d–f** to explore the effect of structural change on the platelet antiaggregating profile. Finally, the influence of the length of the spacer between the heteroaromatic 1,3-benzodioxole and furane rings on the molecular recognition by target bioreceptor was investigated through the planning of the vinylogous analogues **9g–h** and their corresponding *N*-methyl derivatives **9i–j**. Previous results showed that NAH derivatives displayed their platelet aggregating actions mainly through the blockage of thromboxane A_2 (TXA_2) production[8]. These actions at arachidonic acid (AA) metabolism level seem to be dependent on the relationship between NAH framework and the bis-allyl unit of this unsaturated fatty acid[7].

Methods

Chemistry

Melting points were determined using a Quimis instrument and are uncorrected. ^{1}H-NMR spectra were determined otherwise in dimethylsulfoxide (DMSO)-d_6 containing ~1% tetramethylsilane as an internal standard, with Bruker DPX-200 or Bruker DRX-300 spectrometers at 200 or 300 MHz, respectively. ^{13}C-NMR spectra were determined in the same spectrometers described above at 50 or 75 MHz, employing the same solvents. Infrared spectra were obtained using a Nicolet Magna IR 760 spectrometer. Samples were examined as potassium bromide (KBr) disks. Microanalysis was obtained with Thermofinnigan EA1112 analyzer, using a Metler MX5 electronic balance. Reactions were routinely monitored by thin-layer chromatography (TLC) in silica gel (F245 Merck plates), and the products were visualized using iodine or ultraviolet lamp (254 and 365 nm). Column chromatography purifications were performed using silica gel Merck 230–400 mesh. Unless stated otherwise, starting materials used were high-grade commercial products. All organic solutions were dried over anhydrous sodium sulphate, filtered, and concentrated, under reduced pressure, in rotary evaporators.

Methyl 3,4-methylenedioxybenzoate 12

To a solution of piperonal **11** (5.0 g, 33.3 mmol) in absolute methanol (190 ml) cooled at 0°C, were successively added solutions of KOH (5.6 g, 99.9 mmol) in absolute methanol (190 ml) and iodine (10.98 g, 43.2 mmol) in absolute methanol (380 ml) at 0°C. After stirring for 1.5 h at 0°C, small amounts of saturated $NaHSO_3$ solution were added until the disappearance of the brown colour. Next, the methanol was almost totally evaporated under reduced pressure. To the residue was added cold water, and the precipitate formed was filtered out affording the title compound in 80% yield, as a white solid, m.p. 53°C [Lit. (16) 53°C]. See analytical data in supplementary material.

3,4-Methylenedioxybenzoylhydrazine 13

To a solution of the ester **12** (6.42 g, 35.6 mmol) in 25 ml of ethanol, was added 32.5 ml of 80% hydrazine monohydrate. The reaction mixture was maintained under reflux for 3.5 h, when TLC indicated the end of the reaction. Then the media was poured on ice and the resulting precipitate was filtered out affording the title compound in 73% yield, as a white solid, m.p. 170–171°C [Lit. (16) 170–171°C]. See analytical data in supplementary material.

General procedure for preparation of 3,4-methylenedioxybenzoylhydrazones 9a–c and 9g–h

To a solution of 0.150 g (0.83 mmol) of the hydrazine **13** in absolute ethanol (20 ml) containing three drops of 37% hydrochloric acid, was added 0.87 mmol of the corresponding functionalized furfural. The mixture was stirred at room temperature for 30 min, until extensive precipitation was visualized. Next, the solvent was partially concentrated at reduced pressure and the resulting mixture was poured into cold water. The precipitate formed was filtered out and dried under reduced pressure to give the desired NAH derivatives, as described next.

2-Furfurylidene-3,4-methylenedioxybenzoylhydrazine 9a

This compound was obtained as a beige solid by condensation of **13** with furfural in 94% yield, m.p. 215–216°C [Lit. (11) 215–216°C]. See analytical data in supplementary material.

5-Nitro-2-furfurylidene-3,4-methylenedioxybenzoylhydrazine 9b

This compound was obtained as a yellow solid by condensation of **13** with 5-nitro-furfural in 90% yield, m.p. 233–234°C. ^{1}H-NMR (DMSO-d_6; 300 MHz) δ 12.07 (s, CO-N<u>H</u>), 8.37 (s, N=C<u>H</u>), 7.77(d, Furan-H_3', J = 3.5 Hz), 7.54 (d, Ar-H_6, J = 8.0 Hz), 7.44 (s, Ar-H_2), 7.23 (d, Ar-H_4, J = 3.5 Hz), 7.05 (d, Ar-H_5, J = 8.0 Hz), 6.13 (s, O-C<u>H</u>$_2$-O); ^{13}C-NMR (DMSO-d_6; 75 MHz) δ 162.9 (<u>C</u>=O), 152.3 (Furan-C_5'), 151.0 (Ar-C_4), 147.9 (Ar-C_3), 135.5 (N=<u>C</u>H), 126.9 (Ar-C_1), 123.7 (Ar-C_6), 115.6 (Furan-C_4'), 115.1 (Furan-C_3'), 108.6 (Ar-C_5), 108.2 (Ar-C_2), 102.4 (O-<u>C</u>H_2O); IR (KBr, cm^{-1}) 3291 (N-H), 1661 (C=O), 1607 (C=N), 1513.2–1472.0 (NO_2), 1256 (C-O). Elemental Analysis (CHN) Calculated: C, 51.49; H, 2.99; N, 13.86. Found: C, 51.42; H, 2.93; N, 13.75.

5-Bromo-2-furfurylidene-3,4-methylenedioxybenzoylhydrazine 9c

This compound was obtained as a beige solid by condensation of **13** with 5-bromo-furfural in 92% yield, m.p. 155–156°C. See analytical data in supplementary material.

2-Furylpropenylidene-3,4-methylenedioxybenzoylhydrazine 9g

This compound was obtained as a beige solid by condensation of **13** with 3-(2-furyl)acrolein in 51% yield, m.p. 222–223°C. See analytical data in supplementary material.

5-Nitro-2-furylpropenylidene-3,4-methylenedioxybenzoylhydrazine 9h

This compound was obtained as a brown solid by condensation of **13** with 5-nitro-3-(2-furyl)acrolein in 50% yield, m.p. 241–242°C. See analytical data in supplementary material.

General procedure for selective N-methylation of 3,4-methylenedioxybenzoylhydrazones 9a–c and 9g–h

To a solution of 0.75 mmol of corresponding acylhydrazone derivative and 0.31 g (2.25 mmol) of K_2CO_3 in 4 ml acetone, was added 1.5 mmol of CH_3I. The reaction mixture was maintained under reflux for 3 h, when TLC indicated the end of the reaction. To the reaction mixture was added 5 ml of acetone and the mixture was filtered out. The residual solid was washed with 20 ml of acetone and the suspension was filtered. Then, the organic layer was concentrated under reduced pressure to give the desired *N*-methyl-*N*-acylhydrazone derivatives **9d–f** and **9i–h**, as described next.

(2-Furfurylidene)-N-methyl-3,4-methylenedioxybenzoylhydrazine 9d

This compound was obtained as a beige solid by the *N*-methylation of **9a** in 91% yield, m.p. 115–116°C [Lit. (11) 104–105°C]. See analytical data in supplementary material.

N-Methyl-(5-nitro-2-furfurylidene)-3,4-methylenedioxybenzoylhydrazine (LASSBio-1215) 9e

This compound was obtained as a yellow solid by the *N*-methylation of **9b** in 67% yield, m.p. 175–176°C. ^{1}H-NMR (DMSO-d_6; 300 MHz) δ 7.98 (s, N=C<u>H</u>), 7.73 (s, Furan-H_4'), 7.31–7.24 (m, Ar-H_2 and Ar-H_6), 6.99–6.92 (m, Furan-H_3' and Ar-H_5), 6.10 (s, O-C<u>H_2</u>-O), 3.32 (N-C<u>H_3</u>); ^{13}C-NMR (DMSO-d_6; 75 MHz) δ 168.6 (<u>C</u>=O), 152.6 (Ar-C_4), 149.2 (Furan-C_5'), 147.8 (Ar-C_3), 146.4 (Furan-C_2'), 128.5 (N=<u>C</u>H), 127.5 (Furan-C_3'), 125.4 (Furan-C_4'), 114.7 (Ar-C_1), 113.6 (Ar-C_6), 110.3 (Ar-C_2), 107.2 (Ar-C_5), 101.5 (O-<u>C</u>H_2O); 29.5 (N-<u>C</u>H_3); IR (KBr, cm^{-1}) 3451 (N-H), 1670 (C=O), 1604 (C=N), 1521.7–1457.2 (NO_2), 1259 (C-O). Elemental Analysis (CHN) Calculated: C, 53.00; H, 3.49; N, 13.24. Found: C, 53.07; H, 3.55; N, 13.12.

(5-Bromo-2-furfurylidene)-N-methyl-3,4-methylenedioxybenzoylhydrazine 9f

This compound was obtained as a beige solid by the *N*-methylation of **9c** in 83% yield, m.p. 135–137°C. See analytical data in supplementary material.

(2-Furylpropenylidene)-N-methyl-3,4-methylenedioxybenzoylhydrazine 9i

This compound was obtained as a beige solid by the *N*-methylation of **9g** in 92% yield, m.p. 109–110°C. See analytical data in supplementary material.

N-Methyl-(5-nitro-2-furylpropenylidene)-3,4-methylenedioxybenzoylhydrazine 9j

This compound was obtained as a beige solid by the *N*-methylation of **9h** in 79% yield, m.p. 241–242°C. See analytical data in supplementary material.

Pharmacology

Collagen, sodium arachidonate, 9,11-dideoxy-11α,9α-epoxy methanoprostaglandin F2α (U-46619), platelet-activating factor (PAF), ADP, DMSO, acetylsalicylic acid (ASA) were purchased from Sigma Chem. Co. (USA). Indomethacin was purchased from Merck (USA). Thromboxane B_2 enzyme immuno-assay kit was purchased from Amersham Bioscience.

Animals

New Zealand white rabbits weighing 2.5–3.0 kg of both sexes were obtained from the LASSBio breeding unit (Faculty of Pharmacy, UFRJ, Brazil). All animals were kept under standardized conditions, maintained in a 12-h light/dark cycle with water and food ad libitum until use. Animal experiments were performed according to the 'Principles of Laboratory Animal Care and Use in Research' (Colégio Brasileiro de Experimentação Animal-COBEA/Instituto Brasileiro Carlos Chagas Filho-IBCCF, Brazil), based on international guidelines for the care and use of laboratory animals.

Human volunteers

Blood samples were obtained from healthy volunteers who had no apparent thromboembolic or hemorrhagic diseases, renal, hepatic, or malignant conditions, and had not taken any medication for at least 2 weeks prior to blood collection, following their informed consent and approval by the local ethics committee.

Rabbit and human platelet-rich plasma preparation

The rabbit and human blood were obtained by puncture of the central ear artery and by vein puncture of the median cubital vein, respectively, into 3.8% trisodium citrate (9:1 v/v) solution. Platelet-rich plasma (PRP) was prepared by centrifugation at 500×g for 10 min at room temperature. The platelet pour plasma (PPP) was prepared by centrifugation of the pellet at 1800×g for 10 min at room temperature. Platelet count was adjusted to 6×10^8 platelets/ml and 3×10^8 platelets/ml for rabbit and human PRP, respectively.

Platelet aggregation studies

Platelet aggregation was conducted by the turbidimetric method of Born and Cross[17] and monitored using a

platelet lumi-aggregometer (Model 560CA, Chrono-log Corporation, Harvertown, PA, USA). PRP (400 µl) was incubated at 37°C for 1 min with continuous stirring at 1200 rpm. Aggregation of PRP was induced by ADP (5 µM), collagen (5 µg/ml), AA (200 µM), U-46619 (3 µM), and PAF (1 µM).

Test compounds and the vehicle (0.5% DMSO) were added to the PRP samples 5 min before the addition of the aggregating agent. DMSO used as vehicle did not have either pro- or antiplatelet aggregation activity. On the one hand, the platelet antiaggregating activity was expressed as % of inhibition of aggregation induced by ADP, AA, U-46619, and PAF. On the other hand, for collagen-induced aggregation, it was expressed as % inhibition of maximum rate of aggregation (slope).

TXB_2 measurements

TXB_2 levels were measured in human PRP samples submitted to aggregation induced by AA (500 µM) as described above. The TXB_2 formation reaction was stopped by indomethacin 10 µM and ethylenediaminotetraacetic acid (EDTA) 2 mM 5 min after the AA addition. Plasma samples were then centrifuged at 3600×g for 5 min. Supernatant samples were collected and stored in Eppendorf tubes at –20°C. TXB_2 production was determined using an enzyme immuno-assay kit according to the manufacturer's instructions[18,19].

Statistical analysis

Results were expressed as mean ± SEM of independent experiments carried out in duplicate and compared with vehicle control groups. Data were statistically analyzed by the Student's *t*-test or analysis of variance (ANOVA) one-way (Dunnet posttest) for a significance level of $P < 0.05$. When appropriate, the IC_{50} values (i.e., the concentration able to inhibit 50% of the maximum effect observed) were determined by nonlinear regression using GraphPad Prism software v. 4.0.

Results and discussion

Chemistry

The novel series of 1,3-benzodioxole *N*-acylhydrazone derivatives **9** were prepared by applying classical synthetic methodologies exploiting piperonal **11**, obtained from isomerization and oxidative cleavage of safrole **10**[15], as starting material (Scheme 1). The desired key-intermediate (acylhydrazine, **13**) was prepared from aromatic aldehyde **11** in 75% yield (two steps), exploiting the initial oxidation to the corresponding methyl ester **12** followed by acylation of hydrazine, as described previously[11,16]. The target NAH derivatives **9a–c** and **9g–h** were prepared through the acid catalyzed condensation of **13** with the corresponding functionalized furaldehydes **14a–e**[11,16], as depicted in Scheme 1 (see Supplementary Table S1).

The careful analysis of the imine hydrogen shifts on ^{1}H-NMR spectra of all these NAH derivatives allowed us to evidence that they were obtained as a single geometrical isomer at imine double bound level, which were characterized as presenting relative (*E*)-configuration taking on basis the previous crystallographic studies performed with thienyl-NAH derivatives **7** and **8**[11]. The diastereoselective profile of the imine bond formation was also representatively confirmed in acylhydrazone derivative **9a** by using mass spectrometry as auxiliary tool[20], through the appearance of the fragment ($m/z = 165$, relative abundance 21%) of McLafferty rearrangement, which is formed due to the favourable orientation between the carbonyl oxygen atom and the γ-hydrogen in the (*E*)-diastereomer (Figure 3).

Moreover, the vinylogous derivatives **9g–j** presented the same relative configuration (*E*) derived from α,β-unsaturated 2-furaldehydes **14d** and **14e** used at the condensation step with acylhydrazine **13**. The ^{1}H-NMR spectra of these 2-furylpropenylidene NAHs **9g–j** showed a typical AB pattern ($J = 15.9$ Hz) resulting from vicinal coupling between the vinylic hydrogens with the expected (*E*)-configuration.

Finally, the *N*-methyl-NAH derivatives **9d–f** and **9i–j** were obtained from selective alkylation of the corresponding *N*-acylhydrazones **9a–c** and **9g–h** after initial treatment with potassium carbonate in acetone followed by addition of methyl iodide (Scheme 1).

The structure of all furyl *N*-acylhydrazone or *N*-methyl-NAH derivatives described herein was completely characterized by usual spectroscopic methods (see experimental section) before the investigation of their antiplatelet properties.

Pharmacological assays

The *in vitro* activity of the functionalized furfurylidene NAH and *N*-methyl-NAH derivatives (**9**) was evaluated on rabbit platelet aggregation model with AA (200 µM), collagen (5 µg/ml), and adenosine 5-diphosphate (ADP, 5 µM) as the inducers (Table 1)[17]. As a general trend, NAH derivatives **9a–j** showed to be more active as inhibitors of AA-induced platelet aggregation, when compared with the two other exploited agonists. The best antiplatelet profile was evidenced for *N*-methyl nitrofuryl NAH derivative **9e**, which presented an IC_{50} of 0.7 and 4.5 µM in AA- and collagen-induced platelet aggregation, respectively.

Moreover, all unsubstituted NAH derivatives **9a–c**, **9g–h** were less active as platelet antiaggregating agents than the corresponding *N*-methyl NAH derivatives **9d–f**, **9i–j**, possibly indicating that alkylation could change the conformational behaviour of these compounds, as previously described for LASSBio-294 **7** and LASSBio-785 **8**[11]. On the contrary, homologation of NAH framework with a vinyl group does not improve or reduce the antiplatelet activity displayed by the corresponding NAH or *N*-methyl-NAH derivative, as could be evidenced through the comparison of the IC_{50} value of compounds **9e** vs. **9j**, that is 0.7 and 23.2 µM in AA-induced assay, respectively (Table 1).

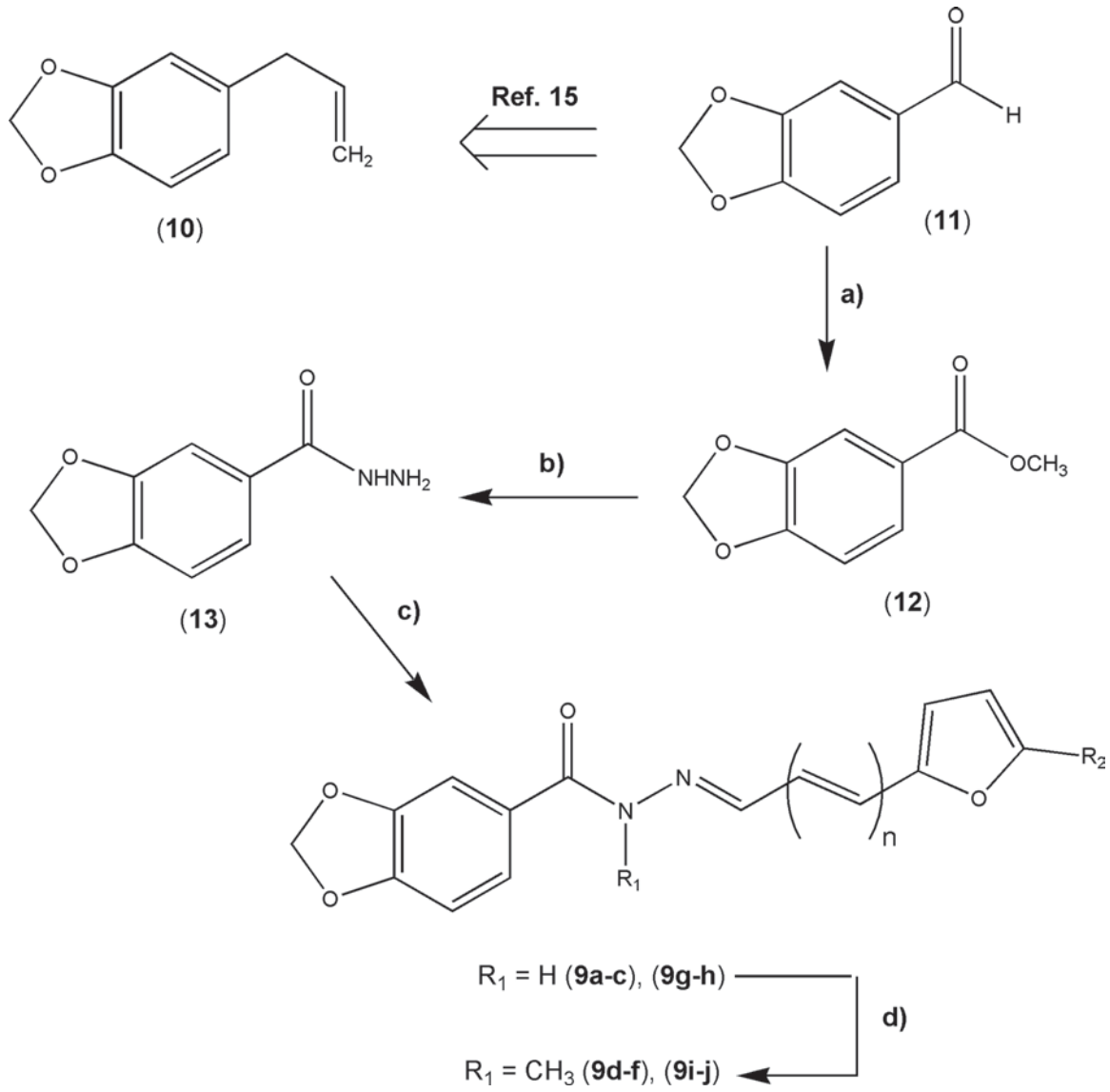

Scheme 1. Reaction conditions: **a)** I_2, KOH, MeOH, rt, 6 h, 90%; **b)** $NH_2NH_2.H_2O$ 80%, EtOH, reflux, 3.5 h, 84%; **c)** Functionalized 2-furyl-$(CH{=}CH)_n$-CHO (**14a–e**), EtOH, rt, 30 min, see Table 1; **d)** K_2CO_3, acetone, MeI, 40°C, 24 h, see supplementary Table S1.

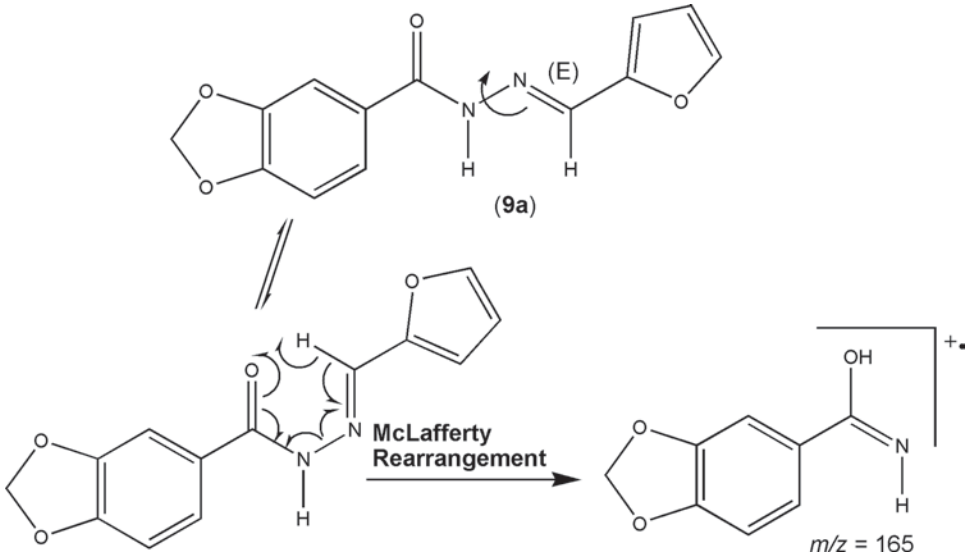

Figure 3. McLafferty rearrangement peak in the mass spectra of (*E*)-(2-furfurylidene) 3,4-methylenedioxybenzoylhydrazine derivative **9a**.

Since the distinct biological profile of derivatives **9b**, **9e**, and their corresponding vinylogous analogues **9h** and **9j** could be associated with their different conformations, we decided to investigate their comparative conformational behaviour through molecular modelling studies.

In this context, their structures were built using SPARTAN 8.0 software[21] and full geometrically optimized using the standard molecular mechanics force field followed by systematic conformational analysis performed using Hartree-Fock 3-21G(*) method[22]. Supplementary Figure S4 shows that minimum energy conformer of NAH derivatives **9b** and **9h** presented antiperiplanar arrangement between carbonyl and N-H bond of amide moiety, whereas in *N*-methyl-NAH derivatives **9e** and **9j** the geometry adopted is mainly synperiplanar between carbonyl and N-CH_3 groups (11), changing the general conformation from a linear to a folded conformation, which contributes to improve the antiplatelet potency.

The comparison of the lowest energy conformations of 5-nitrofuryl compounds **9e** and **9j** with respect to the influence of the spacer unit between the NAH moiety and the heteroaromatic unit corroborates the importance of maintaining an adequate distance and orientation between the groups attached to NAH moiety, the pharmacophore, once the introduction of vinyl group does not present a favourable influence on the platelet antiaggregating activity (Figure S4).

It is interesting to observe that the introduction of hydrophobic bromo substituent at C-5 position of the furan ring of **9c** improves the platelet antiaggregating profile in unsubstituted NAH series, whereas its effect on *N*-methyl NAH series was less pronounced than hydrophilic and H-bond acceptor nitro group, as could be evidenced by the respective antiplatelet potency order, that is **9c**>**9a**>**9b** vs. **9e**>**9d**>**9f**.

Similar structure–activity relationships were found in platelet aggregation induced by collagen, allowing us to distinguish two groups of compounds taking into account the observed antiplatelet potency, that is a group formed by the *N*-methyl-NAH derivatives **9d**, **9e**, **9f**, and **9i** with IC_{50} ranging from 4 to 8 μM and a second one constituted by compounds **9c** and **9j**, which presented IC_{50} of 47.7 and 41.2 μM, respectively. On the contrary, only 5-nitro-furyl-NAH derivatives **9e** and **9j** were able to inhibit moderately the platelet aggregation induced by ADP in rabbit PRP (25.7% and 22.6%, respectively) at 100 μM concentration (Table 1).

Aiming to better understanding the molecular mechanisms associated with the antiplatelet profile of NAH and *N*-methyl-NAH derivatives, the most active compounds **9a**, **9c–9f**, **9i**, and **9j** were evaluated on *in vitro* human platelet aggregation induced by ADP (3 μM) (Table 2). In this assay is observed a characteristic second wave of aggregation, dependent on ADP concentration, which is associated with TXA_2 production, that is almost completely inhibited by ASA or other COX-1 inhibitors, for example indomethacin[18,23].

Despite only compounds **9c** and **9e** have inhibited significantly in 30% and 38%, respectively, the platelet aggregation induced by ADP in human PRP, most of the furyl NAH derivatives were able to block completely the second wave of this process (Table 2). The exceptions were derivatives **9a** and **9j**, which also were not significantly active against ADP. This profile indicates that platelet antiaggregating activity exhibited by these compounds is related to their ability to modulate AA cascade enzymes responsible for TXA_2 biosynthesis, for example COX-1, isoform predominantly on platelets, or thromboxane synthase (TXS).

None of the NAH or *N*-methyl-NAH derivatives **9** was able to inhibit significantly the first wave of platelet aggregation, suggesting that their antiplatelet actions are

Table 1. Effect of functionalized 2-furyl *N*-acylhydrazone derivatives **9a–j** on platelet aggregation induced by arachidonic acid (AA), collagen, and ADP in rabbit platelet-rich plasma.

	IC_{50} values[a] (μM) or inhibition (%) at 100 μM		Inhibition (%) at 100 μM
Compound[b]	Arachidonic acid (200 μM)	Collagen (5 μg/ml)	ADP (5 μM)
Indomethacin	0.6[c]	3.1[c]	—
9a	30.1 (29.8–30.4)	156.1 (114.4–212.9)	14.1
9b	0.0%	3.2%	15.2
9c	7.9 (6.2–10.2)	47.7 (39.7–57.3)	15.0
9d	1.2 (0.4–3.4)	8.2 (6.0–11.1)	2.2
9e	0.7 (0.6–1.1)	4.5 (3.9–5.1)	25.7*
9f	2.0 (1.9–2.2)	6.0 (4.9–7.4)	18.7
9g	47.4 (43.8–51.3)	17.7%	15.6
9h	11.4%	2.1%	18.3
9i	1.7 (0.9–3.1)	6.1 (4.3–8.5)	1.4
9j	23.2 (23.1–23.4)	41.2 (32.7–51.7)	22.6*
LASSBio-294	15.3[c]	18.3[c]	14.7[c]

[a]n = Three independent experiments in duplicate; 95% confidence interval for IC_{50} values is shown in parentheses. [b]*N*-acylhydrazone derivatives **9a–j** were incubated with platelet-rich plasma 5 min before the addition of the agonist (AA, collagen, or ADP) . [c]Data obtained from reference ([8]). *$P < 0.05$ (ANOVA one-way; Dunnet posttest).

Table 2. Effect of ASA and functionalized 2-furyl *N*-acylhydrazone derivatives **9a**, **9c–e**, and **9i–j** on platelet aggregation induced by ADP (3 μM) in human platelet-rich plasma.

				Inhibition (%)	
Compound[a]	*n*[b]	Aggregation[c] (%)	Total inhibition (%)	First wave	Second wave
ADP	4	64.0 ± 4.4	—	—	—
DMSO	4	69.3 ± 7.8	—	—	—
ASA	3	53.0 ± 5.5	23.5	–4.0 n.s.	96.5*
9a	4	58.0 ± 6.0	16.2	–0.5 n.s.	41.7*
9c	4	48.5 ± 3.0	30.0*	0.5 n.s.	88.3*
9d	4	52.5 ± 6.0	24.5	–2.9 n.s.	96.1*
9e	4	42.5 ± 3.8	38.6*	9.7 n.s.	97.4*
9f	4	55.8 ± 6.6	19.5	–8.8 n.s.	94.7*
9i	4	55.5 ± 3.8	19.9	–4.4 n.s.	97.0*
9j	4	69.0 ± 7.6	0.4	–7.9 n.s.	22.4
LASSBio-294	—	—	40.9[d]	—	—

[a]Compounds were assayed at 100 μM concentration. [b]*n* = number of independent experiments in duplicate. [c]Results are expressed as mean ± SEM. [d]Data obtained from reference ([8]). *N*-acylhydrazone derivatives **9** were incubated with plasma-rich platelet 5 min before the addition of the ADP. *$P < 0.05$ (ANOVA one-way; Dunnet posttest).

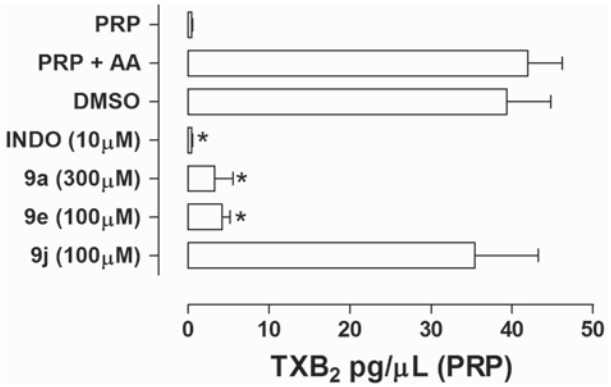

Figure 4. Effect of NAH derivatives **9a**, **9e**, and **9j** on the TXB_2 production in arachidonic acid (500 μM)-induced platelet aggregation in human PRP. Results are expressed in terms of mean ± SEM ($n = 3$–5 independent experiments). *$P < 0.05$ (ANOVA one-way; Dunnet posttest); *N*-acylhydrazone derivatives **9** were incubated with plasma-rich platelet 5 min before the addition of AA; The vehicle concentration in the samples does not exceed 0.3%; INDO = indomethacin.

not related to the blockage of purinergic P2Y1 or P2Y12 receptors ([24]).

Furthermore, in order to confirm the action of some of these NAH derivatives on AA metabolism, we performed studies on the biosynthesis of TXA_2 in the activated human PRP by measuring the production of their stable metabolite TXB_2 ([19]).

Compounds (**9d**) and (**9e**) were selected to this study due to their antiplatelet potency in both rabbit and human platelets. Compound (**9j**) was also elected because of its ability to completely inhibit the platelet aggregation induced by AA in rabbit PRP, although it has not inhibited the second wave of platelet aggregation induced by ADP in human PRP.

The results depicted in Figure 4 showed that compounds LASSBio-1003 **9d** and LASSBio-1215 **9e** at 100 μM were able to inhibit by 92% and 90%, respectively, the production of TXB_2 in human platelets activated by AA (500 μM). Similarly, nonselective COX inhibitor indomethacin (10 μM), used as standard, inhibited almost completely the TXB_2 biosynthesis in this experiment.

On the contrary, vinylogous *N*-methyl-NAH derivative **9j** does not inhibit significantly the production of TXB_2 (Figure 4), indicating that its antiplatelet profile should be dependent on a different mechanism of action those of COX-1 or TXS blockage.

Moreover, none of the NAH derivatives **9a–j** (100 μM) was able to interfere with the rabbit PRP aggregation induced by U-46619 (3 μM) (e.g., vehicle 60.8 ± 1.8 × **9e** 52.1 ± 2.8) or PAF (1 μM) (e.g., vehicle 71.2 ± 1.4 × **9e** 70.3 ± 1.8), indicating that their antiplatelet effects are not dependent of TP or PAF receptor antagonism.

Conclusions

We described herein the discovery of (*E*)-*N*-methyl-*N*'-((5-nitrofuran-2-yl)methylene)benzo[*d*][1,3]dioxole-5-carbohydrazide **9e**, named LASSBio-1215, as a novel antiplatelet agent belonging to the *N*-methyl-*N*-acylhydrazone class, which exert their antiaggregating actions on human and rabbit platelets induced by different agonists, through COX-1 or TXS inhibition. This compound was elected for further pharmacological evaluation on *in vivo* thromboembolic disease models to confirm its potential as a drug candidate for treatment of different cardiovascular disorders and these results will be described in a forthcoming paper.

Declaration of interest

The authors thank CAPES (BR), CNPq (BR), FAPERJ (BR), PRONEX (BR), and INCT-INOFAR (BR, #573.564/2008-6) for financial support and fellowships. The authors report no declarations of interest.

References

1. Murray CJ, Lopez AD. Mortality by cause for eight regions of the world: Global Burden of Disease Study. Lancet 1997;349:1269–1276.
2. Apostolakis S, Shantsila E, Lip GY. Evidence guided antiplatelet treatment: time to move from bench to bedside. Thromb Res 2009;124:649–650.
3. Shore-Lesserson L. Platelet inhibitors and monitoring platelet function: implications for bleeding. Hematol Oncol Clin North Am 2007;21:51–63.
4. Heeschen C, Hamm CW. Difficulties with oral platelet glycoprotein IIb/IIIa receptor antagonists. Lancet 2000;355:330–331.
5. Siddique A, Butt M, Shantsila E, Lip GY. New antiplatelet drugs: beyond aspirin and clopidogrel. Int J Clin Pract 2009;63:776–789.
6. Todeschini AR, Miranda ALP, Silva KCM, Parrini SC, Barreiro EJ. Synthesis and evaluation of analgesic, antiinflammatory and antiplatelet properties of new 2-pyridylaryl-hydrazone derivatives. Eur J Med Chem 1998;33:189–199.
7. Silva GA, Costa LM, Brito FC, Miranda AL, Barreiro EJ, Fraga CA. New class of potent antinociceptive and antiplatelet 10H-phenothiazine-1-acylhydrazone derivatives. Bioorg Med Chem 2004;12:3149–3158.
8. Brito FC, Kummerle AE, Lugnier C, Fraga CA, Barreiro EJ, Miranda AL. Novel thienylacylhydrazone derivatives inhibit platelet aggregation through cyclic nucleotides modulation and thromboxane A2 synthesis inhibition. Eur J Pharmacol 2010;638:5–12.
9. Gonzalez-Serratos H, Chang R, Pereira EF, Castro NG, Aracava Y, Melo PA et al. A novel thienylhydrazone, (2-thienylidene)3,4-methylenedioxybenzoylhydrazine, increases inotropism and decreases fatigue of skeletal muscle. J Pharmacol Exp Ther 2001;299:558–566.
10. Silva AG, Zapata-Sudo G, Kummerle AE, Fraga CA, Barreiro EJ, Sudo RT. Synthesis and vasodilatory activity of new N-acylhydrazone derivatives, designed as LASSBio-294 analogues. Bioorg Med Chem 2005;13:3431–3437.
11. Kümmerle AE, Raimundo JM, Leal CM, da Silva GS, Balliano TL, Pereira MA et al. Studies towards the identification of putative bioactive conformation of potent vasodilator arylidene N-acylhydrazone derivatives. Eur J Med Chem 2009;44:4004–4009.
12. Fraga CA, Barreiro EJ. Medicinal chemistry of N-acylhydrazones: new lead-compounds of analgesic, antiinflammatory and antithrombotic drugs. Curr Med Chem 2006;13:167–198.
13. Rollas S, Küçükgüzel SG. Biological activities of hydrazone derivatives. Molecules 2007;12:1910–1939.
14. Duarte CD, Barreiro EJ, Fraga CA. Privileged structures: a useful concept for the rational design of new lead drug candidates. Mini Rev Med Chem 2007;7:1108–1119.
15. Barreiro EJ, Fraga CAM. The utilization of the safrole, principal chemical constituent of sassafras oil, in the synthesis of compounds actives in the arachidonic acid cascade: antiinflammatory, analgesic and antithrombotic. Quim Nova 1999;22:744–759.
16. Lima PC, Lima LM, da Silva KC, Léda PH, de Miranda AL, Fraga CA et al. Synthesis and analgesic activity of novel N-acylarylhydrazones and isosters, derived from natural safrole. Eur J Med Chem 2000;35:187–203.
17. Born GVR, Cross MJ. The aggregation of blood platelets. J Physiol 1963;168:178–195.
18. Jin J, Quinton TM, Zhang J, Rittenhouse SE, Kunapuli SP. Adenosine diphosphate (ADP)-induced thromboxane A(^{2}) generation in human platelets requires coordinated signaling through integrin alpha(IIb)beta(^{3}) and ADP receptors. Blood 2002;99:193–198.
19. Chou TC, Li CY. Inhibitory mechanisms of dantrolene on platelet aggregation. Thromb Res 1999;96:299–307.
20. Pereira AS, Violante FA, Aquino-Neto FR, Cardoso JN, Fraga CAM, Barreiro EJ, Diastereomeric analysis of bioactive *N*-phenylpyrazole-4-acylhydrazone derivatives by high resolution gas chromatography. Anal Lett 1998;31:719–731.
21. Wavefunction Inc., Irvine, CA, 2000 (license number: DQAIR263775).
22. Binkley JS, Pople JA, Hehre WJ. Self-consistent molecular orbital methods. 21. Small split-valence basis sets for first-row elements. J Am Chem Soc 1980;102:939–947.
23. Smith JB, Ingerman C, Kocsis JJ, Silver MJ. Formation of prostaglandins during the aggregation of human blood platelets. J Clin Invest 1973;52:965–969.
24. Hollopeter G, Jantzen HM, Vincent D, Li G, England L, Ramakrishnan V et al. Identification of the platelet ADP receptor targeted by antithrombotic drugs. Nature 2001;409:202–207.